1   *PDO-driven interdecadal variability of snowfall over the Karakoram and Western Himalaya*

3   **Authors: Priya Bharati[1], Pranab Deb[1], Kieran M. R. Hunt[2,3]**

6   **1 Centre for Ocean, River, Atmosphere and Land Sciences (CORAL), Indian Institute of**

7   **Technology Kharagpur, Kharagpur, India**

8   **2 Department of Meteorology, University of Reading, Reading, UK**

9   **3 National Centre for Atmospheric Science, University of Reading, UK**

12   *Correspondence to*: pranab@coral.iitkgp.ac.in

Abstract:

Our study reveals that the negative phase of the Pacific Decadal Oscillation (PDO-) leads to increased winter (DJF) snowfall in the Karakoram and Western Himalayas (KH) from 1940 to 2022. Interdecadal variations in DJF snowfall during the PDO- are attributed to deep convection and adiabatic cooling near the tropopause in both the northwest Pacific and KH region. Additionally, a wave-like pattern characterized by a trough (anomalous cyclone) north of KH and a ridge (anomalous Tibetan Plateau anticyclone) east of KH in the upper atmosphere, along the northward shift of the DJF Subtropical Jet (STJ) was observed. A strong positive correlation between DJF STJ strength and DJF snowfall in KH as well as a significant negative correlation between DJF STJ strength and DJF PDO, suggests a wave response over KH to the direct forcing over the northwest Pacific Ocean. The intensified STJ across KH results in higher frequency of Western disturbances, leading to anomalous moisture convergence and increased DJF precipitation in the region during the PDO-. These findings hold significant implications for the decadal predictability of winter snowfall in KH by the various phases of PDO.

1) Introduction:

Glaciers in the Karakoram and Western Himalaya (KH) exhibit unique stability compared to other alpine glaciers (known as the 'Karakoram Anomaly'; Hewitt, 2005; Kaab et al., 2012; Gardelle et al., 2013; Kapnick et al., 2014; Forsythe et al., 2017; de Kok et al., 2018; Farinotti et al., 2020; HIMAP, 2020). Winter snowfall plays a significant role in preserving the local snowpack and sustaining the glacial mass balance at higher elevations (Tahir et al., 2011; Bolch et al., 2012; Ridley et al., 2013; Cannon et al., 2015; Dimri et al., 2015), and controls almost 60% of the variability in glacier mass balance in the KH region (Kumar et al., 2019). The decline in average and minimum summer temperatures, along with significant increases in winter, summer, and annual precipitation, have been proposed as crucial factors influencing the stable glacier budget of the KH in recent decades (Archer and Fowler, 2006; Forsythe et al., 2017).

The KH receives around 50% of its annual precipitation as snowfall from western disturbances (WDs) (Lang and Barros, 2004; Barros et al., 2006; Bookhagen and Burbank, 2010; Hunt et al., 2024). Furthermore, WDs account for more than 65% of all winter snowfall and nearly 53% of total winter precipitation in the KH (Javed et al., 2022). However, using a less conservative method, Midhuna et al. (2020) found that WDs account for about 80% of winter precipitation in KH. WDs are upper-level troughs in the subtropical westerly jet (STJ), which grow via baroclinic instability

64 (Norris et al., 2015; Cannon et al., 2017; Hunt et al., 2018). Strong WDs are associated with deep

65 uplift to the east of their centre and drive moist lower-tropospheric southwesterlies from the Arabian

66 Sea (Dimri and Dash, 2012; Hunt et al., 2018), resulting in heavy precipitation along the foothills

67 and mountains of KH region (Baudouin et al., 2020). The snowfall from WDs in the KH is heavily

68 influenced by the complex topography of the region, as well as by synoptic and mesoscale factors

69 (Cannon et al., 2015; Norris et al., 2015, 2017, 2018). Subsequent snowmelt in the following spring

70 and summer seasons and associated runoff serve as major sources of downstream river flow and

71 provide relief from drought to populations that are vulnerable to water stress (Bolch et al., 2012;

72 Hewitt et al., 2014; Rana et al., 2019; Pritchard et al., 2019).

73

74 However, the main climatic drivers affecting seasonal precipitation, and hence glacial mass balance

75 in the region are only partially understood (Cannon et al., 2015). WD activity during winter season

76 over the KH has been reported to be influenced by several global climate forcings such as North

77 Atlantic Oscillation/Arctic Oscillation (Yadav et al., 2009; Syed et al., 2010; Filippi et al., 2014;

78 Basu et al., 2017; Midhuna and Dimri, 2019; Hunt and Zaz, 2022), El Niño–Southern Oscillation

79 (ENSO) (Yadav et al., 2010; Dimri, 2013; Kar and Rana, 2014; Cannon et al., 2017; Kamil et al.,

80 2019; Rana et al., 2019; Bharati et al., 2024), Polar/Eurasian Pattern and Siberian High (Wu and

81 Wang, 2002; Cannon et al., 2014), Madden–Julian Oscillation (Barlow et al., 2005; Cannon et al.,

82 2017) and Indian Ocean Dipole (IOD) (Yadav et al., 2007; Hoell et al., 2013) on intraseasonal and

83 interannual timescales. In particular, the ENSO exerts the strongest influence on the interannual

84 variability of winter precipitation in KH (Rana et al., 2019). One of the key aspects of ENSO

85 teleconnection to Indian Himalayas is the southward shift in the latitude of the winter STJ over the

86 KH during the positive phase of ENSO (Cannon et al., 2014, 2017), which leads to heavier WD

87 precipitation as their tracks move closer to their primary moisture source, the Arabian Sea (Bharati

88 et al., 2024).

89

90 Precipitation gauges in the Himalayas are sparse and recognised as inadequate for accurately

91 measuring snowfall (Anders et al., 2006; Rana et al., 2015). While satellite records of precipitation

92 are available, they cover only a limited time frame, whereas our study requires long-term data to

93 analyse the interdecadal variability of precipitation over the KH region. We currently have an 85-

94 year-long reanalysis from ERA5, which has demonstrated a high degree of similarity in both the

95 quantity and variability of winter precipitation across all time scales when compared to observations

and satellite data in the KH region (Baudouin et al., 2020). The long dataset from ERA5 is sufficient to examine the interdecadal variability of DJF snowfall over KH. The low-frequency modes of atmospheric variability such as the Pacific Decadal Oscillation (PDO), Inter-decadal Pacific Oscillation (IPO) (Mantua et al., 1998; Zhang et al., 1997; Power et al., 1999; Deser et al., 2004; Dai, 2013), and the Atlantic Multi-decadal Oscillation (AMO) (Enfield et al., 2001) are known to modulate the regional climate of the Northern Hemisphere over inter-decadal to multi-decadal timescales. Among these, the PDO is the dominant mode of SST oscillation in the North Pacific, influencing long-term precipitation patterns globally (Dettinger et al., 1998; Krishnamurthy, 2013, 2014; Wang et al., 2014; Dong and Dai, 2015; Yang et al., 2017; Wu and Mao, 2016; Qin et al., 2017; Aggarwal et al., 2023). For example, Indian monsoon rainfall and autumn precipitation in North Central China were found to have an inverse relationship with PDO (Krishnan and Sugi, 2003; Krishnamurthy, 2014; Qin et al., 2017). According to Aggarwal et al. (2023), the PDO has a stronger positive correlation with pre-monsoon precipitation in the northwest Himalayas compared to the ENSO and IOD, leading to a significant decrease in precipitation in recent decades. However, there remains a significant gap in our understanding of the PDO's impact on precipitation over the Himalayas during both monsoon and non-monsoon seasons.

The current study aims to address this knowledge gap by examining the modulation of the interdecadal variability of winter snowfall over KH by PDO. Our study aims to understand the potential influence of the PDO on the Karakoram anomaly, which deviates from the general climate change patterns observed in the KH region and other mountainous areas. The main objective of this study are: (1) To examine the spatial distribution of decadal snowfall in KH in different phases of PDO, (2) how the PDO adjusts global circulation patterns, leading to changes in the STJ, and (3) how these changes cause impact on a local scale over the KH through WDs and moisture transport.

2) Data and Methods:

2.1 Data

2.1.1) Meteorological data

The study uses meteorological data including geopotential height, zonal (u) and meridional wind (v) at 200 hPa level, vertically averaged temperature from 500 to 300 hPa level, vertically integrated moisture flux (VIMF), vertically integrated moisture flux convergence (VIMFC), and global sea

surface temperature (SST) obtained from the European Centre for Medium-Range Weather Forecasts (ECMWF) ERA5 reanalysis from 1940 to 2022. The jet latitude and strength are computed by 200 hPa zonal winds over the region (50º – 80ºE, 10º – 60ºN). The jet latitude is the mean of the latitudes with the largest value of u for each longitude and jet strength is the mean value of u along these latitudes. ERA5 data have global coverage at hourly frequency and a horizontal resolution of 0.25°.

2.1.2) Precipitation data

Precipitation in the KH is mainly observed through satellite derived and reanalysis products (Bosilovich et al., 2008; Joshi et al., 2012; Ménégoz et al., 2013; Palazzi et al., 2013; Rana et al., 2015; Kishore et al., 2016; Baudouin et al., 2020) due to limited and unreliable observations from ground stations in this complex topographical region (Anders et al., 2006; Bookhagen and Burbank 2006; Strangeways, 2010; Rana et al., 2015; Dahri et al., 2018). The ERA5 reanalysis has frequently been used for precipitation and snow in recent studies over the KH (Dahri et al., 2018; Baudouin et al., 2020; T. Singh et al., 2021) and neighbouring mountainous areas (Hu and Yuan, 2020; Li et al. 2021; Dollan et al., 2014). ERA5 closely matches the most reliable gridded measurements over KH in terms of amount, seasonality, and variability across all timescales during winter (Baudouin et al., 2020). However, the accuracy of precipitation datasets varies depending on the season in the region. We choose ERA5 due to its long period, allowing decadal-scale analysis where other datasets do not.

To assess the performance of ERA5 precipitation, we compared the ERA5 precipitation with various gridded precipitation datasets over the KH, including reanalysis datasets from ECMWF ERA5-land, Modern Era Retrospective-analysis for Research, Applications version 2 (MERRA2), and High Asia Refined analysis version 2 (HAR v2), as well as rain gauge, and satellite data from Climate Research Unit version 7 (CRU_TS v7), Global Precipitation Climatology Center version 2022 (GPCC), Global Precipitation Climatology Project version 3.2 (GPCP v3.2), Asian Precipitation - Highly-Resolved Observed Data Integration Towards Evaluation (APHRODITE MA_v1101), CPC-Merged Analysis of Precipitation (CMAP), Tropical Rainfall Measuring Mission (TRMM) Multi-satellite Precipitation Analysis (TMPA) 3B43, and Global Precipitation Measurement mission-Integrated Multi-satellite Retrievals version 7 (GPM_IMERG v7).

We computed the linear correlation coefficient between area-averaged precipitation over the KH region (cropped by the shapefile of the traditional boundaries of the Karakoram-Western and

159 Central Himalaya; highlighted by a green box in Fig. 2a&b) in ERA5 and numerous other

160 precipitation datasets. A strong correlation was seen between DJF ERA5 precipitation and rain-

161 gauge-based precipitation products, including GPCC, GPCP, and CRU, with the exception of

162 CMAP, which exhibited a correlation coefficient of 0.51 (Table 1). All reanalysis products,

163 including ERA5 exhibit similar DJF precipitation variability as seen in observational and satellite

164 datasets over the KH region. The variability of ERA5 precipitation in the KH region aligns closely

165 with all available gridded datasets, despite the presence of biases in ERA5 precipitation across this

166 region. Since most of DJF precipitation in KH occurs as snowfall (Fig. 1b), we utilize ERA5

167 snowfall data to examine the decadal variability of snowfall in the KH (73º – 78ºE, 33º – 38º N).

168 **Table:1 Correlation coefficients of DJF precipitation based on monthly reanalysis, rain-gauge**

169 **and satellite with ERA5 precipitation**

	Name	Time	Spatial resolution	Correlation with ERA5	Source
Reanalysis	ERA5-land	1980-2022	0.25°	0.99	Hersbach et al., 2018
	HAR v2	1980-2020	0.1°	0.92	Wang et al., 2021
	MERRA2	1980-2022	0.5°	0.94	Gelaro et al., 2017
Rain-gauge based	CRU_TS v7	1980-2022	0.5°	0.84	Harris et al., 2014
	GPCC v2022	1980-2020	2.5°	0.89	Schneider et al., 2018
	GPCP	1998-2022	2.5°	0.89	Adler et al., 2016
	CMAP	1980-2022	2.5°	0.51	Xie and Arkin, 1997
	APHRODITE	1998-2015	0.25°	0.67	Yatagai et al., 2012
Satellite	GPM_IMERG v07	2000-2022	0.1°	0.86	Huffman et al., 2015

	TRMM 3B43	1998-2019	0.25°	0.85	Huffman et al., 2007

170

2.1.2) PDO index

172 The PDO index from the National Oceanic and Atmospheric Administration National Climate Data
173 Center (NOAA-NDC) (https://www.ncei.noaa.gov/access/monitoring/pdo/) is employed to describe
174 the interdecadal variability of the Pacific Ocean over the period 1940 to 2022.

175

2.1.3) Western disturbance data

177 WD statistics are computed from the WD track catalogue described in Hunt et al., (2018) and
178 Nischal et al., (2022), which is based on ERA5 reanalysis data that is spectrally truncated to T42 to
179 remove noise and small-scale structures. The tracking algorithm detects WDs by identifying upper-
180 tropospheric regions of positive relative vorticity averaged between 450 hPa and 300 hPa, with the
181 locations of candidate WDs identified as centroids of these regions. The candidate WDs are then
182 further refined by only accepting those: 1) whose locations are linked through time to form tracks
183 that generally follow the westerly steering winds associated with the STJ, 2) that persist for at least
184 48 hours, and 3) that pass through north India (50°–77°E, 22°–42.5°N). The northern limit of this
185 box, 42.5ºN, is more poleward than has been used previous studies (36.5ºN). This allows us to
186 better capture WD impacts over the Karakoram.

187

2.2 Methods

2.2.1) Lanczos filter

190 To isolate the decadal signals, we linearly detrended all meteorological variables and the PDO index
191 for DJF. These datasets were then filtered using a 9-year running mean Lanczos filter, which is a
192 low-pass filter based on the sinc convolution (Duchon et al., 1979). The positive (negative) phase of
193 PDO is defined as years when the filtered DJF PDO index is greater than (less than) zero. We define
194 the negative epoch (PDO-) as two negative phases of PDO that occurred from 1948 to 1977 and
195 1989 to 2014, and the positive epoch (PDO+) as a positive phase of PDO that occurred from 1978
196 to 1988 (Fig.1b). Also, the detrended variables are used to conduct correlation and composite

197 analyses. The Student's and Welch's t-test are used in the study to determine the statistical
198 significance of correlation and composite analyses, respectively.

199

200 **2.2.2) Wavelet analysis**

201 The PyCWT library (https://pycwt.readthedocs.io/en/latest/tutorial/cwt/) is used to calculate the
202 cross-wavelet power spectrum. This library is based on the implementation by Torrence and Compo
203 (1998). We employed the cross wavelet transform to calculate the wavelet spectrum between
204 monthly time series of the PDO index and the area averaged monthly ERA5 snowfall over the KH
205 region. The cross wavelet transform finds regions in time frequency space where the time series
206 show high common power.

207

3) Results:

3.1) PDO and KH winter snowfall

210 This study aims to examine the long-term variability in DJF snowfall in the KH region in relation
211 with the PDO from 1940 to 2022. There is a significant negative correlation between the lowpass-
212 filtered and detrended time series of DJF PDO and DJF snowfall in the KH (Fig 1b), with a
213 coefficient of -0.51. However, the PDO is not a single phenomenon, but rather a set of processes
214 that occur in both the tropics and the extratropics and reflects the influence of various processes
215 occurring at distinct timescales (Newman et al., 2016). More precisely, elevated sea surface
216 temperature (SST) in the eastern tropical Pacific is linked to lower SST in the central and western
217 North Pacific, while higher SST is observed in the eastern North Pacific (Deser et al. 2004;
218 Newman et al., 2016). Thus, decadal variability in the North Pacific SSTs is linked to tropical
219 Pacific decadal variability, specifically in terms of the long-lasting seasonal ENSO patterns
220 (Newman et al., 2011; Wittenberg et al. 2014) as well as the ENSO like multidecadal oscillation
221 (i.e., IPO; Zhang et al., 1997). Occasionally, the AMO may also influence multidecadal variability
222 of the PDO (Zhang and Delworth, 2007). After excluding of the influences of ENSO and IPO, the
223 correlation slightly increases to -0.53 and -0.54, and rises to -0.67 upon the elimination of the
224 AMO's impact.

225

226 The spatial structure of the correlation between PDO and KH snowfall in winter (Fig. 2a) is
227 significantly negative along the western and central Himalayas and much of the southern
228 Karakoram, but positive over the Tibetan Plateau and north India. The snowfall in the KH region
229 during the boreal autumn (SON) and spring (MAM) has a strong positive correlation with the PDO
230 (not shown), whereas the summer monsoon season (JJA) displays a weak but positive correlation
231 with the PDO. The different signs of the correlation suggest that the dynamic processes driving KH
232 snowfall either vary by season, or the seasonal influence of the PDO on KH snowfall changes.

233

234 Figure 2b displays the regional distribution of the difference in detrended DJF snowfall between the
235 negative and positive phases of PDO, hereafter referred to as PDO- and PDO+, respectively. The
236 difference is significantly positive in the KH area, particularly over the southern part of the
237 Karakoram region. DJF snowfall in the KH accounts for around 80-90% of total annual snowfall
238 during the time period (not shown). During PDO+, DJF snowfall over KH is nearly 7% lower than
239 the average seasonal snowfall, while during PDO- it is about 6% higher. It indicates that the
240 difference in DJF snowfall in KH varies significantly depending on the phase of the PDO across
241 several decades.

242

243 This strong relationship between PDO and snowfall in the KH is also demonstrated through a cross-
244 wavelet frequency spectrum analysis between the unfiltered monthly time series of PDO index and
245 snowfall over the KH from 1940 to 2022 (Fig. 2c). The band of strong and significant power in the
246 period of ~1 year in the cross-wavelet indicates that the PDO and KH snowfall both have strong
247 interannual variability. The well-known influence of ENSO on snowfall in the region (operating on
248 interannual timescales) during DJF is also slightly modulated by the low-frequency oscillation of
249 PDO. Another band of significant power exists in the 6-15 year range, indicating a high decadal
250 scale correlation between these two time series. The significant power in the 6-15-year range
251 occurred between 1940 and 1970 and again from 1998 to 2015, coinciding with the negative phases
252 of the PDO. An insignificant weak power appeared within the same range from 1971 to 1988,
253 coinciding with the positive phase of the PDO. A long band of strong power exists throughout the
254 16–20-year range, observed from 1950 to 1990, while a weaker power is shown from 2000 to 2022.
255 This indicates that the low-frequency variability of KH snowfall is influenced by decadal
256 oscillations over various time scales, while the interdecadal variability of KH snowfall is found to
257 influenced by the phase of the PDO.

258

3.2) Sea Surface temperature (SST) variability during DJF

Figure 3a illustrates the well-known positive (or warm) phase of the PDO over the North Pacific, shown as a correlation between lowpass filtered and detrended sea surface temperature (SST) and PDO index during DJF. The correlation pattern also reveals a strong El-Nino like pattern in the eastern equatorial-tropical Pacific Ocean. For comparison, the correlation pattern between the DJF SST anomalies and the DJF snowfall anomalies in the KH region is shown in Figure 3b. This correlation strongly resembles the negative (or cool) phase of the PDO over the North Pacific Ocean. It is characterised by positive SST anomalies in the northwest Pacific and negative SST anomalies in the northeast Pacific. Additionally, there are negative SST correlations in the tropical eastern Pacific region and eastern Indian Ocean adjacent to Western Australia, while positive correlations are observed in the southwest Indian Ocean and across the northwest Atlantic Ocean. The correlation pattern in the southern Indian Ocean reveals the subtropical Indian Ocean Dipole signature (positive phase) (Behera & Yamagata, 2001; Yamagami & Tozuka, 2014).

272

3.3) Upper atmosphere circulation response with PDO and snowfall

To understand the anomalous atmospheric circulations that connect the PDO with anomalous DJF snowfall in the KH region, we computed the correlation of 200 hPa geopotential height with both the DJF PDO index (Fig. 4a) and DJF snowfall (Fig. 4b). The correlation pattern between the PDO and upper-level geopotential height shows a prominent upper-level trough over east China, Japan and the northwest Pacific, which is known as East Asian trough (EAT; Qin et al., 2018; Yin and Zhang, 2021). In contrast, the correlation pattern over the Caspian Sea, KH, and Lake Baikal region is associated with positive geopotential height anomalies. The EAT is a well-known upper atmospheric response to the positive phase of PDO to the East Asia-North Pacific region during the Northern Hemisphere winter (Newman et al, 2016; Qin et al., 2018; Yin and Zhang, 2021). The intensity of the EAT is strongly linked to the strength of the winter monsoon in East Asia and the tilt in the EAT axis is connected to midlatitude baroclinic processes, such as the eddy-driven jet or WD tracks over the East Asia-North Pacific region (Wang et al., 2009). Therefore, changes in location and intensity of the EAT can lead to, or otherwise indicate, regional climate anomalies, such as temperature in the upper troposphere which subsequently influence DJF precipitation in East Asia as well as the KH during the positive phase of the PDO.

289   These patterns change sign during negative phases of PDO, when KH snowfall is enhanced,
290   implying an anomalous upper-level trough to the west of the Karakoram, consistent with increased
291   WD frequency or intensity. The correlation between upper-level geopotential height and snowfall
292   has a similar pattern to the PDO-geopotential correlation, but as expected, with reversed sign. The
293   correlation pattern exhibits a strong ridge (or a weakened EAT) over the northwest Pacific and
294   Japan characterised by the significant positive geopotential height anomalies. The negative
295   correlation to the west of the KH area shows a trough, which is stronger than the positive
296   correlation between PDO and geopotential height, indicating the linkage of seasonal snowfall to the
297   passage of WDs is stronger than the link between the PDO and WDs. Both, however, are important.
298   The appearance of the anomalous trough in both pairs of correlations implies that the PDO may
299   affect KH snowfall by somehow modulating WD activity. Therefore, it is essential to understand
300   how decadal fluctuations in DJF snowfall in the KH are driven by WDs and how the PDO
301   influences WD behaviour. This can be accomplished by investigating the DJF STJ, followed by a
302   detailed investigation of the WDs.

303

304   **3.4) Modulation of WD and Subtropical Westerly Jet by the PDO**

305   To further illustrate the above relationship between PDO and DJF snowfall in KH, we examine the
306   composite differences in 200 hPa wind, geopotential height, and temperature (Fig. 5) between PDO-
307   and PDO+. Figure 5a displays the difference in 200 hPa circulation over East Asia, Arabian
308   Peninsula and northwest Pacific region. During the PDO-, there is a large negative geopotential
309   height anomaly to the north of KH region, which extends from the Caspian Sea-Arabian Peninsula
310   to KH. Strong westerlies are observed to the south of this trough with a stronger STJ prevailing
311   across KH during the PDO-. An anomalous trough in the upper atmosphere is indicative of
312   increased WD frequency (or intensity) and the frequency of WDs is strongly affected by variations
313   in both the latitude and intensity of the STJ (Dimri et al., 2015; Hunt et al., 2017, 2018) over South
314   Asia. Therefore, we now focus on understanding the relationship between the PDO and the STJ.

315

316   Upper-level jets are thermal wind responses to upper-level meridional temperature gradients. In Fig
317   5b, we show the difference in mid-to-upper (from 500 hPa to 300 hPa) tropospheric temperature
318   between PDO- and PDO+. A quadrupole in the upper air temperature gradient is present across the
319   KH, Tibetan Plateau (TP) and the northwest Pacific region during PDO-. Over the Pacific, this is
320   effectively a direct response to the anomalous surface heating provided by the PDO. Anomalous

321 warm SSTs over the northwest Pacific lead to adiabatic cooling near the tropopause, which results

322 in deep convection over the Maritime Continent during the PDO- (e.g., Wang et al., 2016).

323 Upstream, over continental Asia, the relationship is more complicated and is probably a wave

324 response to the direct forcing over the ocean. Therefore, a strongly enhanced meridional

325 temperature gradient over the KH and TP, leading to a stronger and more meridionally-locked STJ.

326

327 Figure 5c displays the lowpass filtered time series of latitude and strength of the DJF STJ. During

328 the PDO-, the STJ tends to sit slightly further north but is also substantially stronger. The

329 correlation of the time series of the strength of DJF STJ with DJF PDO is significantly negative (-

330 0.22), and the correlation between DJF STJ strength and DJF snowfall in KH is strong positive

331 (0.51). The positive (negative) phase of the PDO enhances the movement of the STJ towards the

332 south (north) through a response to the decreased (increased) SST over the northwest Pacific and

333 modulates the cyclonic (anticyclonic) circulation over the northwest Pacific and adjacent maritime

334 continents (Matsumura & Horinouchi, 2016). During PDO-, we observed a quadrupole in the

335 anomalous upper-level temperature gradient (Fig. 5b), resulting in a negative anomaly in the

336 temperature gradient and an anticyclonic circulation (Fig. 5a) over the TP. Thus, by modulating the

337 STJ, the negative phase of the PDO leads to more frequent (more intense) WDs at slightly higher

338 latitudes than usual (e.g. into the Karakoram, where the signal is the strongest).

339

340 The presence of a stronger STJ along with a wave-like pattern of trough (anomalous cyclone) over

341 the northern region of KH, and a ridge (anomalous TP anticyclone) in the upper atmosphere,

342 increases the occurrence of WDs over KH during the PDO-. After examining the impact of the PDO

343 on the STJ, we now quantify its influence on WDs directly. Maps of the difference in the frequency

344 of DJF WDs between PDO- and PDO+ (Fig. 6a) indicate that WDs are more frequent (with a 9%

345 higher frequency) over the KH region during PDO- compared to PDO+. Also, the frequency of

346 WDs is found to be reduced by around 3% in both the northern and southern regions of the KH

347 during PDO- compared to PDO+. These WDs are observed to be more intense in the vicinity of the

348 Caspian Sea and north of the KH during PDO- rather than PDO+ (not shown).

349

350 **3.5) Atmospheric-ocean response of PDO on moisture transport in KH**

351 Increased frequency and intensity of WDs have a significant impact on precipitation in the KH and
352 surrounding region because they govern southwesterly moisture transport from the Arabian Sea
353 (Baudouin et al., 2021; Hunt and Dimri 2021). The composite difference of DJF VIMF and VIMFC
354 between PDO- and PDO+ is now examined to determine the response of moisture transport to the
355 PDO and its subsequent effect on the KH (Fig. 6b). The average difference of VIMFC between
356 PDO- and PDO+ is about 0.8×10^{-5} kg m^{-2} s^{-1} within KH region. An advection of moisture from the
357 Black Sea, Red Sea, and eastern Mediterranean Sea through the Arabian Peninsula/Arabian Sea
358 towards the KH in westerly fashion is observed. The precipitation associated with WDs is mostly
359 determined by their intensity and proximity to the Arabian Sea (Baudouin et al., 2020). The
360 variations in the moisture transport across the Arabian Peninsula/Arabian Sea are not directly linked
361 to changes in VIMF over the northwest Pacific, but the presence of more WDs south of the strong
362 DJF STJ over KH clearly result in greater moisture transport towards KH during PDO-. Hence, the
363 anomalous moisture transport nearly perpendicular to KH, results in increased moisture flux
364 convergence about 16% greater during the PDO- compared to the PDO+ and leads to greater
365 precipitation in the region during PDO-.

366

4) Conclusion and Discussion:

368 The recent impacts of climate change over the KH, particularly in mean and extreme winter
369 precipitation, have been largely attributed largely to anthropogenic forcing, such as greenhouse
370 gases, aerosols, and changes in land use. However, these changes cannot be solely explained by
371 natural forcing (Krishnan et al., 2018). Oceanic conditions, especially changes in SSTs over the
372 equatorial-tropical Pacific and north Pacific, play an important role in driving interdecadal
373 variability in atmospheric circulation and hence winter precipitation over the KH.

374

375 DJF snowfall in the KH accounts for around 80-90% of total annual snowfall during the time
376 period, hence a 15% difference in DJF snowfall can have a significant influence on agriculture in
377 this region, especially since most of the rivers in this region, such as tributaries of Indus, Tarim and
378 Ganges are partially fed by snowmelt in the spring and later seasons (Armstrong et al., 2018).
379 Understanding the interdecadal variability and its relationship with the PDO is important for
380 understanding the long-term climate of the KH. We have analysed the long-term variability in
381 winter snowfall over the KH due to PDO by using ERA5 reanalysis data from 1940 to 2022.We
382 found that a strong negative correlation of -0.51 between the PDO and DJF snowfall in the KH.

383 Mean KH snowfall during DJF is approximately 6% greater than the DJF seasonal average during
384 PDO-, and 7% lower during PDO+.

385

386 PDO associated anomalous warming of SST in the northwest Pacific modulates the snowfall in the
387 KH via changes in upper-level temperatures over the Pacific and Asia. The warm SSTs lead to
388 increased deep convection and subsequent upper-tropospheric adiabatic cooling over the Pacific.
389 During PDO-, the anomalous heating of the tropospheric column over North Pacific leads to a wave
390 like pattern with an upper-level trough over the north of KH and upper-level ridge over the Tibetan
391 Plateau. This results in a stronger STJ to the west of, and over, the KH, before it is deflected
392 northwards over the Tibetan Plateau. There is a strong positive correlation between the strength of
393 DJF STJ and DJF snowfall in KH, with a correlation coefficient of 0.51, and a significant negative
394 correlation between the strength of STJ and PDO, with a correlation coefficient of -0.22 during DJF
395 at decadal scale. These results indicate a wave response over KH to the direct forcing of the north
396 Pacific Ocean.

397 These anomalous jet conditions over KH are linked to a higher occurrence of WDs across the
398 region. Using a track catalogue, we found that WDs are 9% more frequent across the KH and drop
399 by approximately 3% in both the northern and southern regions of the KH during PDO- compared
400 to PDO+. However, the WDs are found to be more intense in the vicinity of the Caspian Sea and
401 north of the KH during PDO- rather than PDO+, which is not shown in this study. This increase in
402 WD frequency results in anomalous moisture transport from the Arabian Sea, Black Sea, Red Sea,
403 and eastern Mediterranean Sea towards the KH. The moisture transport is almost perpendicular to
404 the orography of the KH, leading to a strong moisture convergence about 16% greater during the
405 PDO- compared to the PDO+ and thus increased DJF precipitation in the region during the negative
406 phases of the PDO.

407 Our findings highlight the importance of considering interdecadal variability when trying to
408 quantify the effects of anthropogenic climate change in the KH. The recent PDO- has led to
409 increased WD activity, and hence increased winter snowfall over this region, and may be masking
410 the effects of climate change. More research is needed to disentangle climate change from the
411 effects of interdecadal variability over this vulnerable region, so that policymakers can be better
412 informed. The uncertainty in the snowfall and precipitation datasets, along with the limitations of
413 the short timeseries available from reanalysis for examining decadal oscillations, are insufficient to
414 demonstrate such studies. Future long-term climate simulations could be used for subsequent work

415 if the models accurately represent the interaction between the PDO and snowfall/precipitation in
416 this region.

417

418 **5) List of figures:**

419
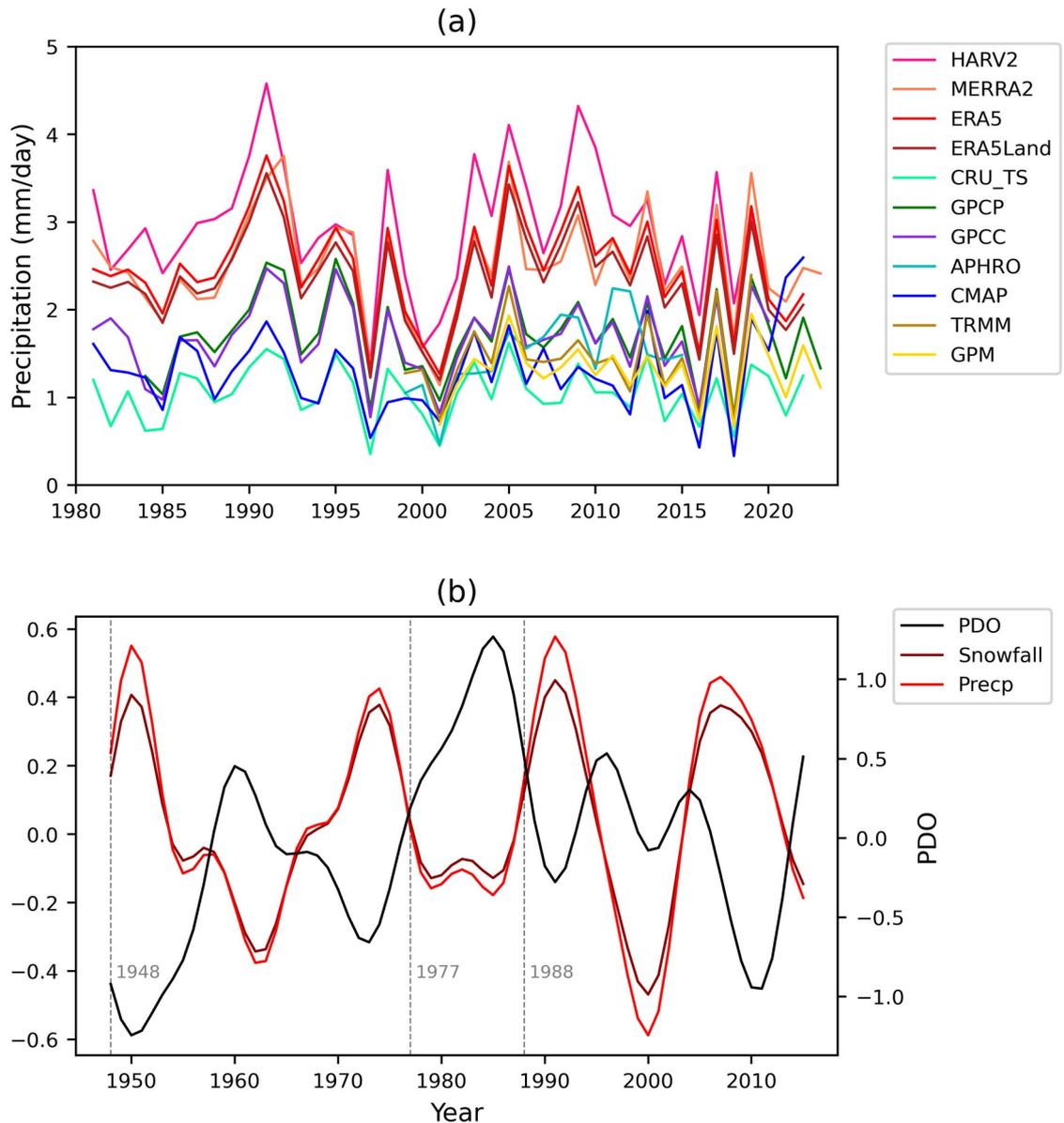
441 **Figure 1: (a) Seasonal variability of DJF precipitation in the KH region (highlighted by a**
442 **green box in Fig. 2a&b; 73º – 78º E, 33º – 38º N) from ERA5, ERA5-land, MERRA2, HARv2,**
443 **CRU_TS, GPCP, GPCC, and CMAP during the period from 1980 to 2020, APHRODITE**
444 **from 1998 to 2015, TRMM from 1998 to 2019, and GPM from 2000 to 2023. (b) Time series of**
445 **9-year filtered DJF PDO index and area-averaged DJF ERA5 snowfall (and precipitation)**

 anomalies over the KH region from 1940 to 2022. The vertical grey lines represent phase

447 **transitions of PDO.**

448
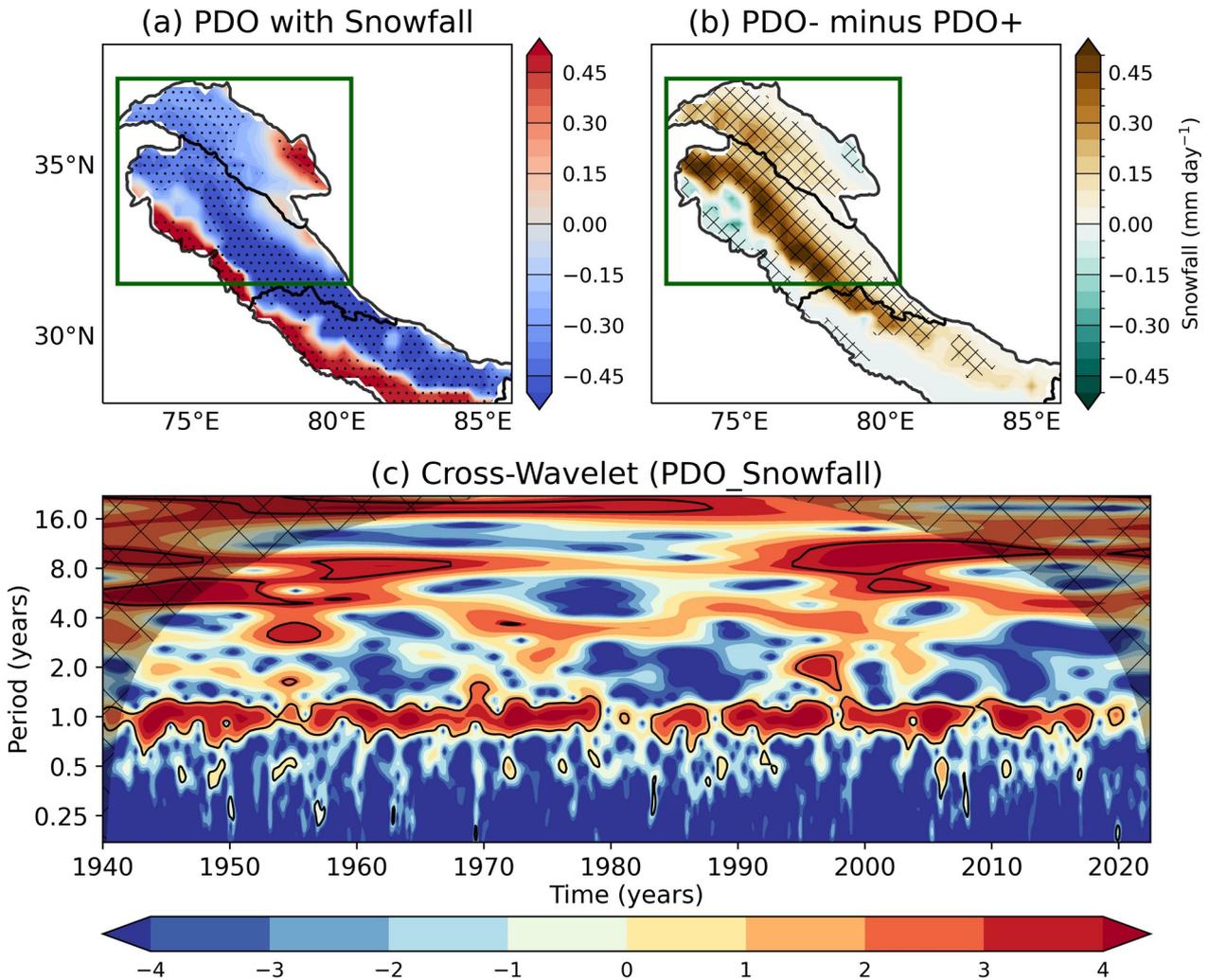
450 **Figure 2: (a) Spatial map of correlation between the 9-year filtered PDO index and the**

451 **snowfall (mm) over the KH region (cropped by the shapefile of the traditional boundaries of**

452 **the Karakoram-Western and Central Himalaya; highlighted by a green box; 73° – 78° E, 33° –**

453 **38° N) during DJF, and (b) composite difference of DJF snowfall (mm) between negative and**

454 **positive epoch of PDO, (c) cross-wavelet of DJF snowfall (mm) over the KH and DJF PDO**

455 **index from 1940 to 2022. Traditional boundaries of Karakoram-Western and Central**

456 **Himalayan regions are marked by thick black lines in (a) and (b). Stippling in (a) and (b)**

457 **denotes regions where the correlation and composite differences are significant at a 95%**

458 **confidence level, as determined by the two-tailed Student's t-test and Welch's t-test,**

respectively. Black line contours on the power spectra in (c) indicate where the spectral power of the cross-wavelet is significantly greater than zero at a 95% confidence level.
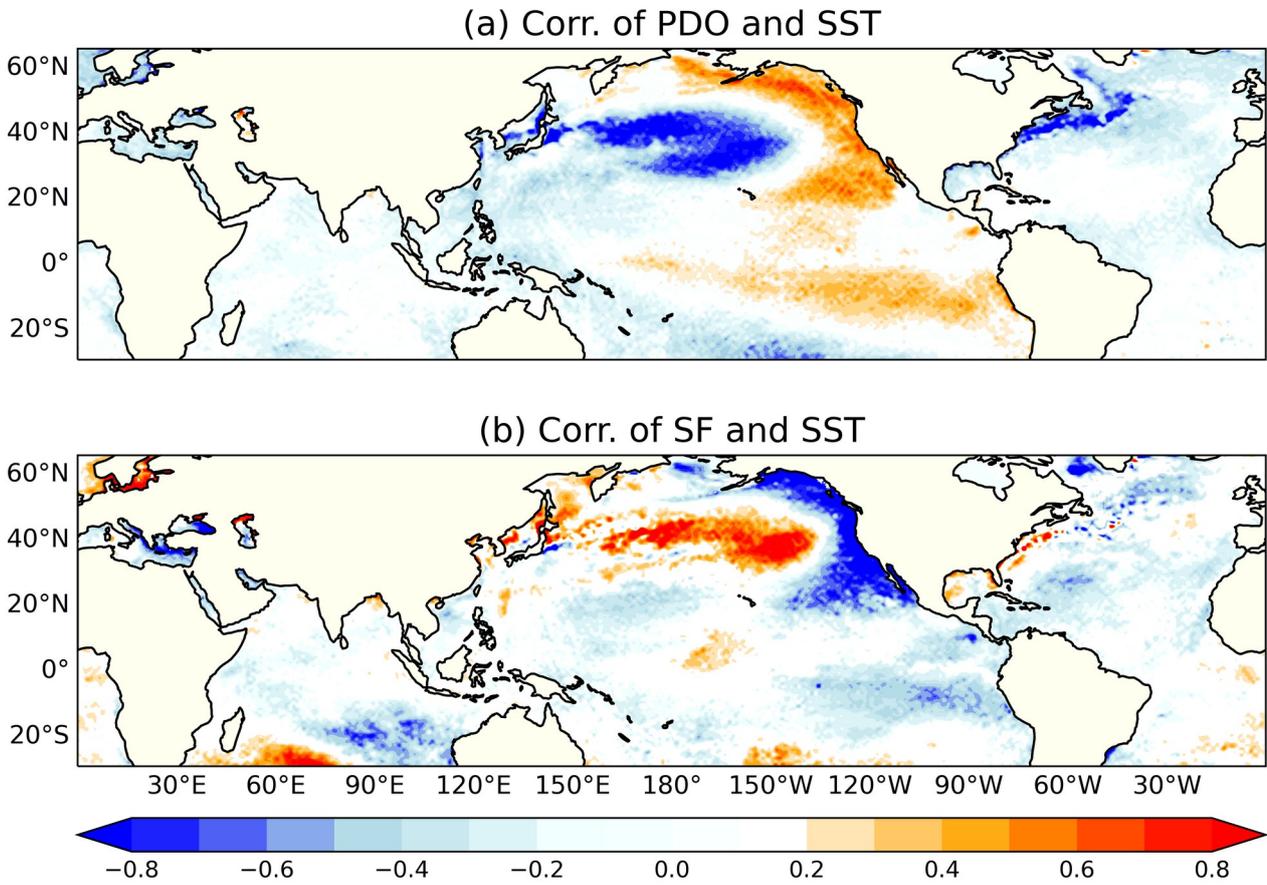
Figure 3: Spatial map of correlation of the 9-year filtered (a) DJF PDO index, and (b) area averaged DJF snowfall over the KH region (as defined in Fig.2) with 9-year filtered DJF sea surface temperature from 1940 to 2022. The correlations patterns are statistically significant at the 95% confidence level, as determined by the two tailed student's t-test.

476
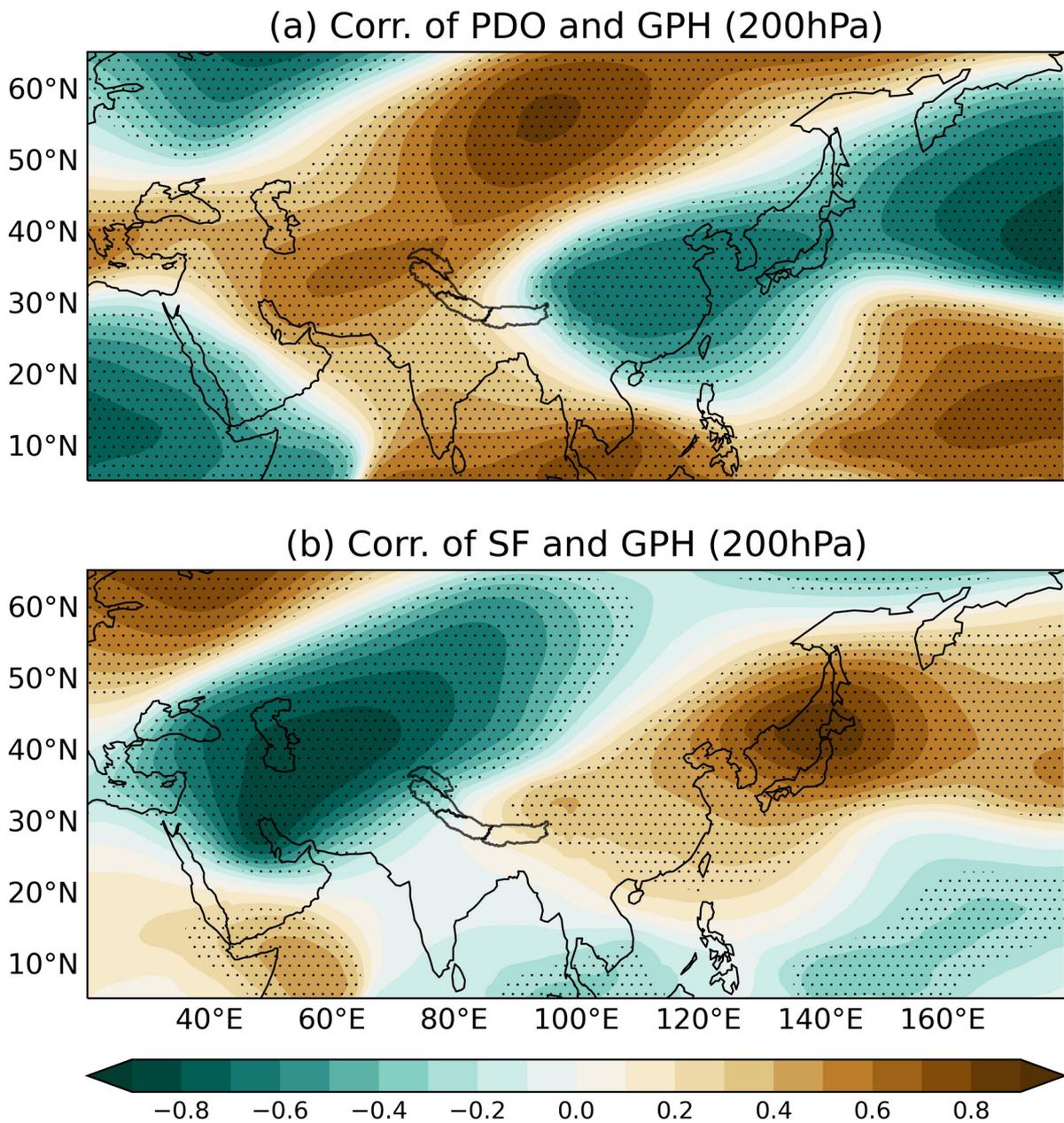
Figure 4: Spatial map of correlation of the 9-year filtered (a) DJF PDO index, and (b) area averaged DJF snowfall (mm) over the KH region (as defined in Fig.2) with 9-year filtered DJF geopotential height at 200hPa (m) from 1940 to 2022. Stippling in (a) and (b) indicate where the correlations are significant at a 95% confidence level, as determined by the two tailed student's t-test.

(a) PDO- minus PDO+

U-wind (200hPa)   → Wind:5 m s^{-1}

(b) PDO- minus PDO+

Temperature (°C)

(c)
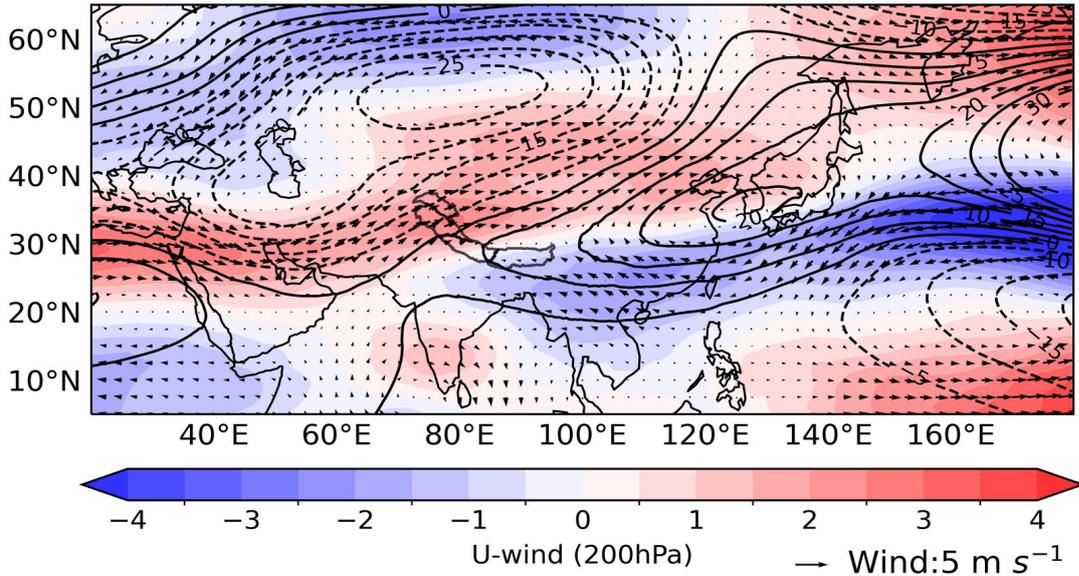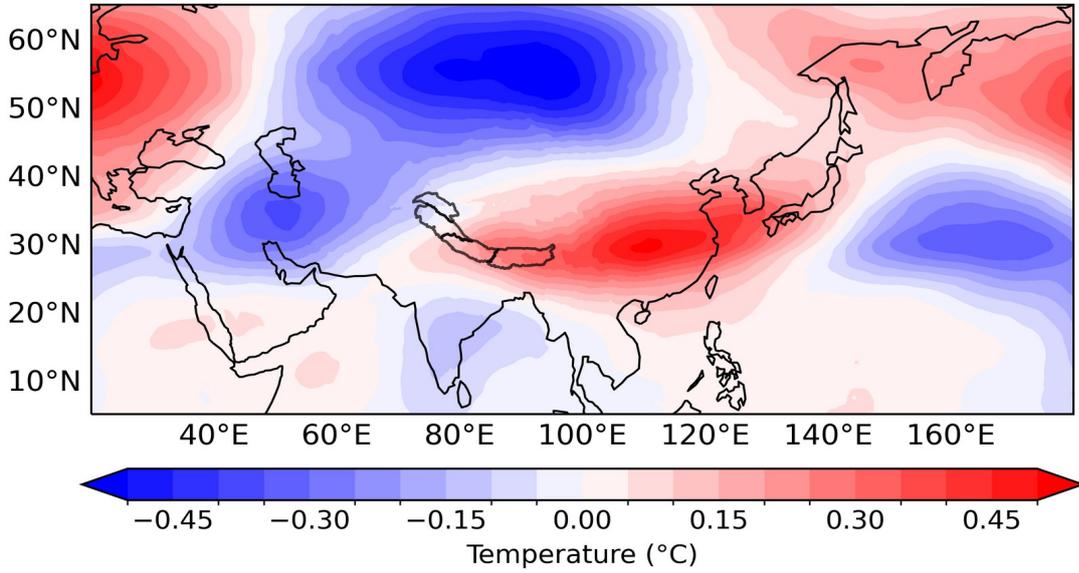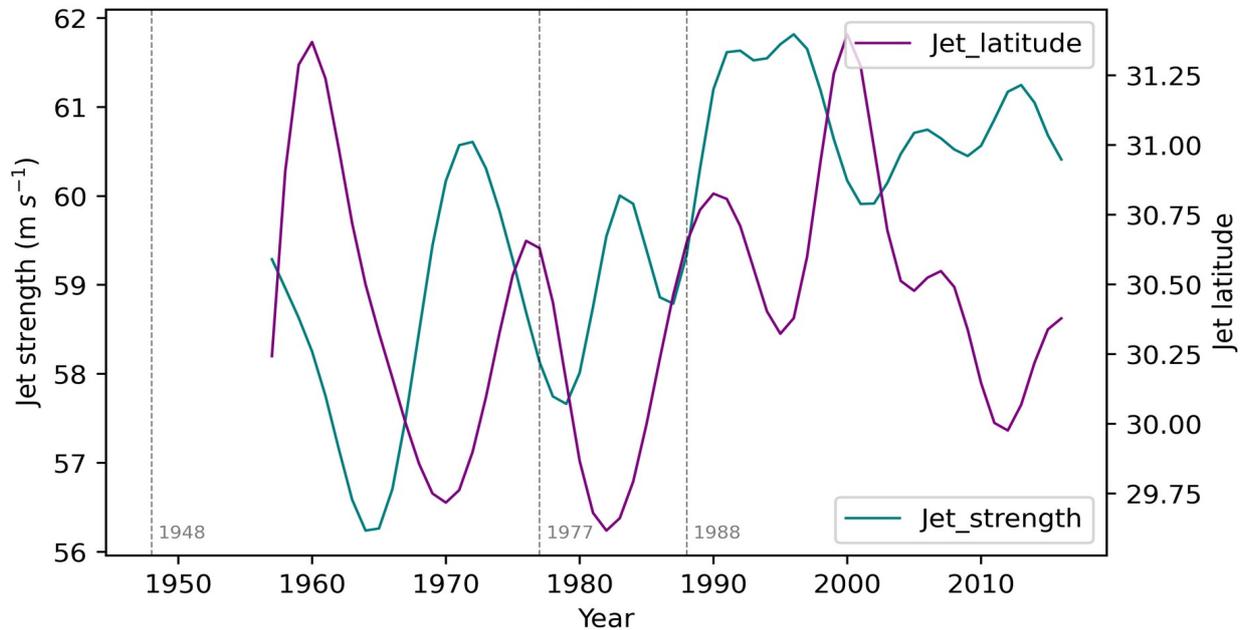
Figure 5: Composite difference of (a) U-wind (colours; m s⁻¹), wind (vectors; m s⁻¹), and geopotential height (contours; m), (b) vertically averaged temperature (ºC) from 300hPa to 500hPa level during DJF between negative and positive epoch of PDO, (c) time series of 9-year filtered strength (magenta; m s⁻¹), and latitude (blue) of DJF subtropical westerly jet over the KH region from 1940 to 2022.
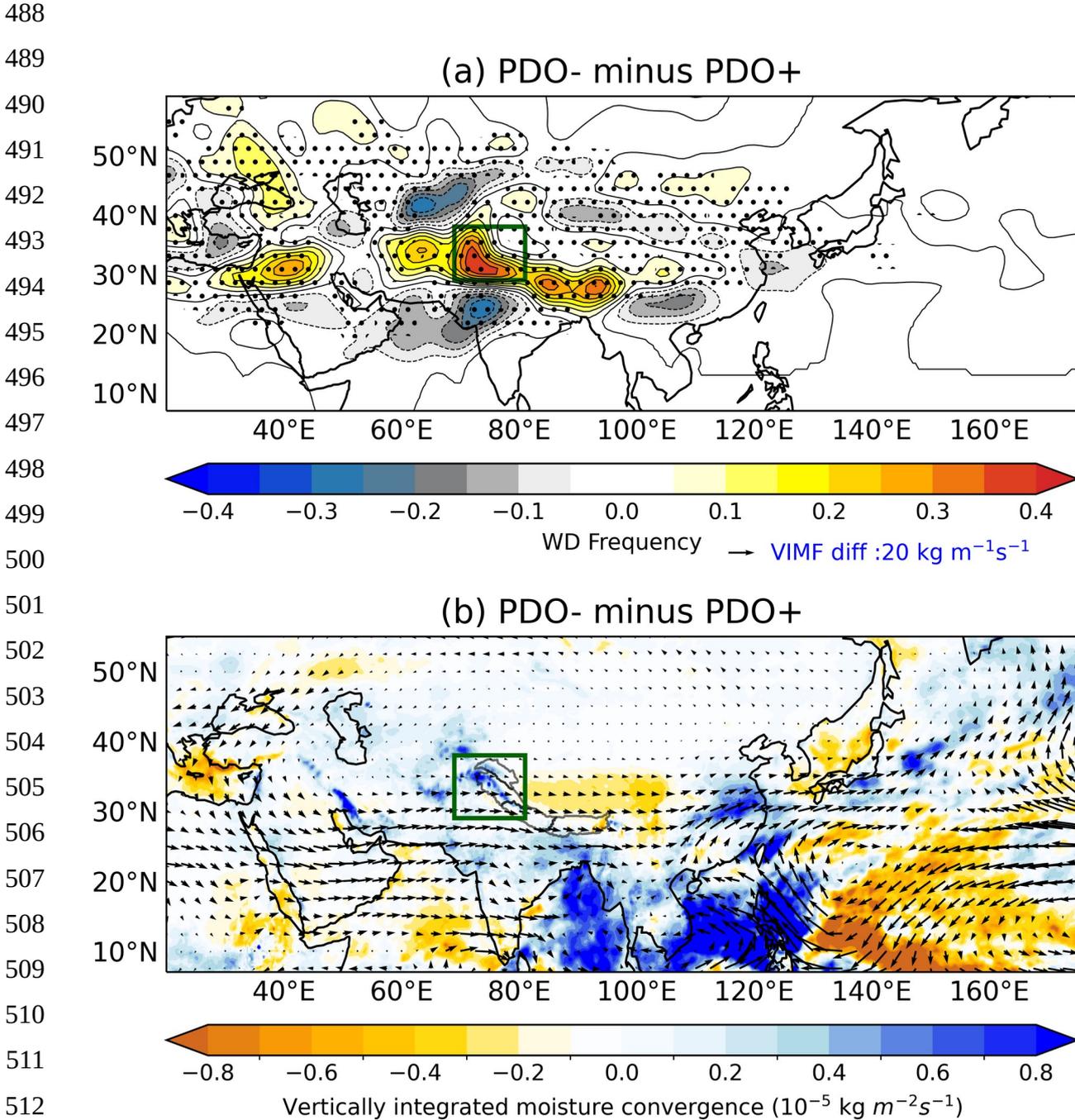
Figure 6: Composite difference of (a) WD frequency, and (b) vertically integrated moisture flux (vectors; kg m⁻¹ s⁻¹) and vertically integrated moisture convergence (colours; kg m⁻² s⁻¹) during DJF between negative and positive epoch of PDO from 1940 to 2022. Stippling in (a)

indicates where the differences are significant at a 95% confidence level, as determined by the two tailed Welch's t-test. **Green box in (a) and (b) highlights the KH region (as defined in Fig.2).**

Author Contributions:

Priya Bharati: conceptualization; formal analysis; methodology; investigation; software; visualization; writing original draft. **Kieran M. R. Hunt:** conceptualization; methodology; software; writing - review and editing. **Pranab Deb:** supervision; conceptualization; writing – review and editing.

Competing interests: The contact author has declared that none of the authors has any competing interests.

Acknowledgements:

The work is carried at CORAL, Indian Institute of Technology Kharagpur under supervision of Pranab Deb. Priya Bharati is funded through the Ministry of Science and Technology, Government of India, Council of Scientific and Industrial Research (CSIR; 09/081(1371)/2019-EMR-I). KMRH is supported by a NERC Independent Research Fellowship (MITRE; NE/W007924/1).

References:

Adler, R., Sapiano, M., Huffman, G., Bolvin, D., Gu, G., Wang, J., and Becker, A.: The new version 2.3 of the Global Precipitation Climatology Project (GPCP) monthly analysis product, University of Maryland, April, 1072-1084, 2016.

Aggarwal, D., Chakraborty R., and Attada, R.: Investigating bi-decadal precipitation changes over the Northwest Himalayas during the pre-monsoon: role of Pacific decadal oscillations, Climate Dynamics, 62(2), 1203-1218, 2024. https://doi.org/10.1007/s00382-023-06969-3

544 Archer, D. R., and Fowler, H. J.: Spatial and temporal variations in precipitation in the Upper Indus
545 Basin, global teleconnections and hydrological implications, Hydrology and Earth System Sciences,
546 8(1), 47-61, 2004. https://doi.org/10.5194/hess-8-47-2004

547

548 Armstrong, R. L., Rittger, K., Brodzik, M. J., Racoviteanu, A., Barrett, A. P., Khalsa, S. J. S., and
549 Armstrong, B.: Runoff from glacier ice and seasonal snow in High Asia: separating melt water
550 sources in river flow, Regional Environmental Change, 19, 1249-1261, 2019.
551 https://doi.org/10.1007/s10113-018-1429-0

552

553 Barlow, M., Wheeler, M., Lyon, B., and Cullen, H.: Modulation of daily precipitation over
554 southwest Asia by the Madden–Julian oscillation, Monthly weather review, 133(12), 3579-3594,
555 2005. https://doi.org/10.1175/MWR3026.1

556

557 Basu, S., Bieniek, P. A., and Deoras, A.: An investigation of reduced western disturbance activity
558 over Northwest India in November-December 2015 compared to 2014-A case study, Asia-Pacific
559 Journal of Atmospheric Sciences,53, 75-83, 2017. DOI:10.1007/s13143-017-0006-7

560

561 Baudouin, J. P., Herzog, M., and Petrie, C. A.: Cross-validating precipitation datasets in the Indus
562 River basin, Hydrology and Earth System Sciences, 24(1), 427-450, 2020.
563 https://doi.org/10.5194/hess-24-427-2020

564

565 Beck, H., Pan, M., Roy, T., and Wood, E. F.: Evaluation of 27 precipitation datasets using Stage-IV
566 gauge-radar data for the CONUS, AGU Fall Meeting 2018, 2018.

567

568 Behera, S. K., and Yamagata, T.: Subtropical SST dipole events in the southern Indian Ocean,
569 Geophysical Research Letters, 28(2), 327-330, 2001. https://doi.org/10.1029/2000GL011451

570

571

572 Bharati, P., Deb, P., Hunt, K., Orr, A., and Dash, M. K.: ENSO-induced latitudinal variation of the
573 subtropical jet modulates extreme winter precipitation over the Western Himalaya, Advances in
574 Atmospheric Sciences. doi: 10.1007/s00376-024-4057-2

575

576 Bolch, T., Kulkarni, A., Kääb, A., Huggel, C., Paul, F., Cogley, J. G., and Stoffel, M.: The state and
577 fate of Himalayan glaciers, Science, 336(6079), 310-314, 2012. DOI: 10.1126/science.1215828

578

579 Bonekamp, P. N., De Kok, R. J., Collier, E., and Immerzeel, W. W.: Contrasting meteorological
580 drivers of the glacier mass balance between the Karakoram and central Himalaya, Frontiers in Earth
581 Science, 7, 107, 2019. https://doi.org/10.3389/feart.2019.00107

582

583 Bookhagen, B., and Burbank, D. W.: Toward a complete Himalayan hydrological budget:
584 Spatiotemporal distribution of snowmelt and rainfall and their impact on river discharge, Journal of
585 Geophysical Research: Earth Surface, 115(F3), 2010. https://doi.org/10.1029/2009JF001426

586

587 Bosilovich, M. G., Chen, J., Robertson, F. R., and Adler, R. F.: Evaluation of global precipitation in
588 reanalyses, Journal of applied meteorology and climatology, 47(9), 2279-2299, 2008.
589 https://doi.org/10.1175/2008JAMC1921.1

590

591 Cannon, F., Carvalho, L. M., Jones, C., and Bookhagen, B.: Multi-annual variations in winter
592 westerly disturbance activity affecting the Himalaya, Climate dynamics, 44, 441-455, 2015. DOI
593 10.1007/s00382-014-2248-8

594

595 Cannon, F., Carvalho, L. M., Jones, C., Hoell, A., Norris, J., Kiladis, G. N., and Tahir, A. A.: The
596 influence of tropical forcing on extreme winter precipitation in the western Himalaya, Climate
597 Dynamics, 48, 1213-1232, 2017. DOI 10.1007/s00382-016-3137-0

598

599   Dahri, Z. H., Moors, E., Ludwig, F., Ahmad, S., Khan, A., Ali, I., and Kabat, P.: Adjustment of
600   measurement errors to reconcile precipitation distribution in the high-altitude Indus basin,
601   International Journal of Climatology 2018; 38: 3842–3860, 2018. DOI: 10.1002/joc.5539

602

603   Dai, A. (2013). The influence of the inter-decadal Pacific oscillation on US precipitation during
604   1923–2010, Climate dynamics, 41(3), 633-646, 2013. DOI 10.1007/s00382-012-1446-5

605

606   de Kok, R. J., Tuinenburg, O. A., Bonekamp, P. N., and Immerzeel, W. W.: Irrigation as a potential
607   driver for anomalous glacier behavior in High Mountain Asia, Geophysical research letters, 45(4),
608   2047-2054, 2018. https://doi.org/10.1002/2017GL076158

609

610   Deser, C., Phillips, A. S., & Hurrell, J. W.: Pacific interdecadal climate variability: Linkages
611   between the tropics and the North Pacific during boreal winter since 1900, Journal of Climate,
612   17(16), 3109-3124, 2004. https://doi.org/10.1175/1520-0442(2004)017<3109:PICVLB>2.0.CO;2

613

614   Dimri, A. P., Niyogi, D., Barros, A. P., Ridley, J., Mohanty, U. C., Yasunari, T., and Sikka, D. R.:
615   Western disturbances: a review, Reviews of Geophysics, 53(2), 225-246, 2015.
616   https://doi.org/10.1002/2014RG000460

617

618   Dimri, A. P., and Dash, S. K.: Wintertime climatic trends in the western Himalayas, Climatic
619   Change, 111, 775-800, 2012. DOI 10.1007/s10584-011-0201-y

620

621   Dimri, A. P., and Niyogi, D.: Regional climate model application at subgrid scale on Indian winter
622   monsoon over the western Himalayas, International Journal of Climatology, 33(9), 2013.

623

624   Dimri, A. P.: Relationship between ENSO phases with Northwest India winter precipitation,
625   International Journal of Climatology, 33(8), 1917-1923, 2013. DOI: 10.1002/joc.3559

626

627   Dollan, I. J., Maina, F. Z., Kumar, S. V., Nikolopoulos, E. I., and Maggioni, V.: An assessment of
628   gridded precipitation products over High Mountain Asia, Journal of Hydrology: Regional Studies,
629   52, 101675, 2024. https://doi.org/10.1016/j.ejrh.2024.101675

630

631   Dong, B., and Dai, A.: The influence of the interdecadal Pacific oscillation on temperature and
632   precipitation over the globe, Clim Dyn, 45, 2667-2681, 2015. DOI 10.1007/s00382-015-2500-x

633

634   Duchon, C. E.: Lanczos filtering in one and two dimensions, Journal of Applied Meteorology and
635   Climatology,   18(8),   1016-1022,   1979.   https://doi.org/10.1175/1520-
636   0450(1979)018%3C1016:LFIOAT%3E2.0.CO;2

637

638   Enfield, D. B., Mestas-Nuñez, A. M., and Trimble, P. J.: The Atlantic multidecadal oscillation and
639   its relation to rainfall and river flows in the continental US, Geophysical research letters, 28(10),
640   2077-2080, 2001. https://doi.org/10.1029/2000GL012745

641

642   Farinotti, D., Immerzeel, W. W., de Kok, R. J., Quincey, D. J., and Dehecq, A.: Manifestations and
643   mechanisms of the Karakoram glacier Anomaly, Nature geoscience, 13(1), 8-16, 2020.
644   https://doi.org/10.1038/s41561-019-0513-5

645

646   Filippi, L., Palazzi, E., von Hardenberg, J., and Provenzale, A.: Multidecadal variations in the
647   relationship between the NAO and winter precipitation in the Hindu Kush–Karakoram, Journal of
648   climate, 27(20), 7890-7902, 2014. https://doi.org/10.1175/JCLI-D-14-00286.1

649

650   Forsythe, N., Fowler, H. J., Li, X. F., Blenkinsop, S., and Pritchard, D.: Karakoram temperature and
651   glacial melt driven by regional atmospheric circulation variability, Nature Climate Change, 7(9),
652   664-670, 2017. DOI: 10.1038/NCLIMATE3361

653

654   Fowler, H. J., and Archer, D. R.: Conflicting signals of climatic change in the Upper Indus Basin,
655   Journal of climate, 19(17), 4276-4293, 2006. https://doi.org/10.1175/JCLI3860.1

656

657 Gardelle, J., Berthier, E., & Arnaud, Y.: Slight mass gain of Karakoram glaciers in the early twenty-
658 first century, Nature geoscience, 5(5), 322-325, 2012. DOI: 10.1038/NGEO1450

659

660 Gelaro, R., McCarty, W., Suárez, M. J., Todling, R., Molod, A., Takacs, L., and Zhao, B.: The
661 modern-era retrospective analysis for research and applications, version 2 (MERRA-2), Journal of
662 climate, 30(14), 5419-5454, 2017. https://doi.org/10.1175/JCLI-D-16-0758.1

663

664 Harris, I. P. D. J., Jones, P., Osborn, T., and Lister, D.: Updated high-resolution grids of monthly
665 climatic observations-the CRU TS3. 10 Dataset, International journal of climatology, 34, 623-642,
666 2014.

667

668 Hersbach, H., de Rosnay, P., Bell, B., Schepers, D., Simmons, A., Soci, C., and Berrisford, P.:
669 Operational global reanalysis: Progress, future directions and synergies with NWP (ERA report
670 Series No. 27), European Centre for Medium Range Weather Forecasts: Reading, UK, 2018.

671

672 Hewitt, K.: The Karakoram anomaly? Glacier expansion and the 'elevation effect,' Karakoram
673 Himalaya, Mountain Research and Development, 332-340, 2005. https://doi.org/10.1659/0276-
674 4741(2005)025[0332:TKAGEA]2.0.CO;2

675

676 Hewitt, K. (2014).: Glaciers of the Karakoram Himalaya, Encyclopedia of Snow, Ice and Glaciers,
677 edited by: Singh, VP, Singh, P., and Haritashya, UK, Springer Netherlands, Dordrecht, 429-436,
678 2014. DOI 10.1007/978-94-007-6311-1

679

680 Hoell, A., Barlow, M., and Saini, R.: Intraseasonal and seasonal-to-interannual Indian Ocean
681 convection and hemispheric teleconnections, Journal of Climate, 26(22), 8850-8867, 2013.
682 https://doi.org/10.1175/JCLI-D-12-00306.1

683

684 Huffman, G. J., Bolvin, D. T., Nelkin, E. J., Wolff, D. B., Adler, R. F., Gu, G., and Stocker, E. F.:
685 The TRMM multisatellite precipitation analysis (TMPA): Quasi-global, multiyear, combined-sensor
686 precipitation estimates at fine scales, Journal of hydrometeorology, 8(1), 38-55, 2007.
687 https://doi.org/10.1175/JHM560.1

688

689 Huffman, G. J., Bolvin, D. T., Braithwaite, D., Hsu, K., Joyce, R., Xie, P., and Yoo, S. H.: NASA
690 global precipitation measurement (GPM) integrated multi-satellite retrievals for GPM (IMERG),
691 Algorithm theoretical basis document (ATBD) version, 4(26), 2020-05, 2015.

692

693 Hunt, K. M., Turner, A. G., and Shaffrey, L. C.: The evolution, seasonality and impacts of western
694 disturbances, Q. J. R. Meteorol. Soc., 144(710), 278-290, 2018. DOI:10.1002/qj.3200

695

696 Hunt, K. M., and Fletcher, J. K.: The relationship between Indian monsoon rainfall and low-
697 pressure systems, Climate Dynamics,53(3), 1859-1871, 2019. https://doi.org/10.1007/s00382-019-
698 04744-x

699

700 Hu, X., and Yuan, W.: Evaluation of ERA5 precipitation over the eastern periphery of the Tibetan
701 plateau from the perspective of regional rainfall events, International Journal of Climatology, 41(4),
702 2625-2637, 2021. DOI: 10.1002/joc.6980

703

704 Hunt, K. M., and Zaz, S. N.: Linking the North Atlantic Oscillation to winter precipitation over the
705 Western Himalaya through disturbances of the subtropical jet, Climate Dynamics, 60(7), 2389-
706 2403, 2023. https://doi.org/10.1007/s00382-022-06450-7

707

708 Hunt, K. M., Baudouin, J. P., Turner, A. G., Dimri, A. P., Jeelani, G., Pooja, and Palazzi, E.: Western
709 disturbances and climate variability: a review of recent developments, EGUsphere,2024, 1-106,
710 2024. https://doi.org/10.5194/egusphere-2024-820

711

712 Javed, A., Kumar, P., Hodges, K. I., Sein, D. V., Dubey, A. K., and Tiwari, G.: Does the recent

713 revival of western disturbances govern the Karakoram anomaly?, Journal of Climate, 35(13), 4383-

714 4402, 2022. DOI: 10.1175/JCLI-D-21-0129.1

715

716 Joshi, M. K., Rai, A., and Pandey, A. C.: Validation of TMPA and GPCP 1DD against the ground

717 truth rain-gauge data for Indian region, International journal of climatology,33(12), 2013. DOI:

718 10.1002/joc.3612

719

720 Kääb, A., Berthier, E., Nuth, C., Gardelle, J., and Arnaud, Y.: Contrasting patterns of early twenty-

721 first-century glacier mass change in the Himalayas, Nature, 488(7412), 495-498, 2012.

722 doi:10.1038/nature11324

723

724 Kamil, S., Almazroui, M., Kang, I. S., Hanif, M., Kucharski, F., Abid, M. A., and Saeed, F.: Long-

725 term ENSO relationship to precipitation and storm frequency over western Himalaya–Karakoram–

726 Hindukush region during the winter season, Climate Dynamics, 53, 5265-5278, 2019.

727 https://doi.org/10.1007/s00382-019-04859-1

728

729 Kapnick, S. B., Delworth, T. L., Ashfaq, M., Malyshev, S., and Milly, P. C.: Snowfall less sensitive

730 to warming in Karakoram than in Himalayas due to a unique seasonal cycle, Nature Geoscience,

731 7(11), 834-840, 2014. DOI: 10.1038/NGEO2269

732

733 Kar, S. C., and Rana, S.: Interannual variability of winter precipitation over northwest India and

734 adjoining region: impact of global forcings, Theoretical and applied climatology, 116, 609-623,

735 2014. DOI 10.1007/s00704-013-0968-z

736

737 Kishore, P., Jyothi, S., Basha, G., Rao, S. V. B., Rajeevan, M., Velicogna, I., and Sutterley, T. C.:

738 Precipitation climatology over India: validation with observations and reanalysis datasets and

739 spatial trends, Clim Dyn, 46, 541-556, 2016. DOI 10.1007/s00382-015-2597-y

740

741 Krishnan, R., Sabin, T. P., Madhura, R. K., Vellore, R. K., Mujumdar, M., Sanjay, J., and Rajeevan,

742 M.: Non-monsoonal precipitation response over the Western Himalayas to climate change, Climate

743 Dynamics, 52, 4091-4109, 2019. https://doi.org/10.1007/s00382-018-4357-2

745 Krishnan, R., and Sugi, M.: Pacific decadal oscillation and variability of the Indian summer

746 monsoon rainfall, Climate Dynamics, 21, 233-242, 2003. DOI 10.1007/s00382-003-0330-8

748 Krishnamurthy, L., and Krishnamurthy, V. J. C. D.: Influence of PDO on South Asian summer

749 monsoon and monsoon–ENSO relation, Climate dynamics, 42, 2397-2410, 2014. DOI

750 10.1007/s00382-013-1856-z

752 Krishnamurthy, L., and Krishnamurthy, V.: Decadal scale oscillations and trend in the Indian

753 monsoon rainfall, Clim Dyn, 43, 319-331, 2014. DOI 10.1007/s00382-013-1870-1

755 Lang, T. J., and Barros, A. P.: Winter storms in the central Himalayas, Journal of the Meteorological

756 Society of Japan. Ser. II, 82(3), 829-844, 2004. https://doi.org/10.2151/jmsj.2004.829

758 Mantua, N. J., Hare, S. R., and Zhang, Y.: A Pacific interdecadal climate oscillation with impacts on

759 salmon production, Oceanographic Literature Review, 1(45), 36, 1998.

761 Ménégoz, M., Gallée, H., and Jacobi, H. W.: Precipitation and snow cover in the Himalaya: from

762 reanalysis to regional climate simulations, Hydrology and Earth System Sciences, 17(10), 3921-

763 3936, 2013. https://doi.org/10.5194/hess-17-3921-2013

766 Midhuna, T. M., and Dimri, A. P.: Impact of arctic oscillation on Indian winter monsoon,

767 Meteorology and Atmospheric Physics, 131, 1157-1167, 2019. https://doi.org/10.1007/s00703-018-

768 0628-z

770 Midhuna, T. M., Kumar, P., and Dimri, A. P.: A new Western Disturbance Index for the Indian
771 winter monsoon, Journal of Earth System Science, 129, 1-14, 2020. https://doi.org/10.1007/s12040-
772 019-1324-1

773

774 Newman, M., Shin, S. I., and Alexander, M. A. Natural variation in ENSO flavors, Geophysical
775 Research Letters, 38(14), 2011. https://doi.org/10.1029/2011GL047658

776

777 Newman, M., Alexander, M. A., Ault, T. R., Cobb, K. M., Deser, C., Di Lorenzo, E., and Smith, C.
778 A.: The Pacific decadal oscillation, revisited, Journal of Climate, 29(12), 4399-4427, 2016. DOI:
779 10.1175/JCLI-D-15-0508.1

780

781 Nischal, Attada, R., and Hunt, K. M.: Evaluating winter precipitation over the western Himalayas in
782 a high-resolution Indian regional reanalysis using multisource climate datasets, Journal of Applied
783 Meteorology and Climatology, 61(11), 1613-1633, 2022. https://doi.org/10.1175/JAMC-D-21-
784 0172.1

785

786 Norris, J., Carvalho, L. M., Jones, C., and Cannon, F.: WRF simulations of two extreme snowfall
787 events associated with contrasting extratropical cyclones over the western and central Himalaya,
788 Journal of Geophysical Research: Atmospheres, 120(8), 3114-3138, 2015.
789 https://doi.org/10.1002/2014JD022592

790

791 Norris, J., Carvalho, L. M., Jones, C., Cannon, F., Bookhagen, B., Palazzi, E., and Tahir, A. A.: The
792 spatiotemporal variability of precipitation over the Himalaya: evaluation of one-year WRF model
793 simulation, Climate Dynamics, 49, 2179-2204, 2017. DOI 10.1007/s00382-016-3414-y

794

795 Norris, J., Carvalho, L. M., Jones, C., and Cannon, F.: Deciphering the contrasting climatic trends
796 between the central Himalaya and Karakoram with 36 years of WRF simulations, Climate
797 Dynamics, 52, 159-180, 2019. https://doi.org/10.1007/s00382-018-4133-3

798

799 Palazzi, E., Von Hardenberg, J., and Provenzale, A.: Precipitation in the Hindu-Kush Karakoram
800 Himalaya: observations and future scenarios, Journal of Geophysical Research: Atmospheres,
801 118(1), 85-100, 2013. https://doi.org/10.1029/2012JD018697

802

803 Power, S., Casey, T., Folland, C., Colman, A., and Mehta, V.: Inter-decadal modulation of the
804 impact of ENSO on Australia, Climate dynamics, 15, 319-324, 1999.

805

806 Pritchard, H. D.: Asia's shrinking glaciers protect large populations from drought stress, Nature,
807 569(7758), 649-654, 2019. https://doi.org/10.1038/s41586-019-1240-1

808

809 Qin, M., Li, D., Dai, A., Hua, W., and Ma, H.: The influence of the Pacific Decadal Oscillation on
810 North Central China precipitation during boreal autumn, International Journal of Climatology, 38,
811 e821-e831, 2018. DOI: 10.1002/joc.5410

812

813 Rana, S., McGregor, J., and Renwick, J.: Precipitation seasonality over the Indian subcontinent: An
814 evaluation of gauge, reanalyses, and satellite retrievals, Journal of Hydrometeorology, 16(2), 631-
815 651, 2015. https://doi.org/10.1175/JHM-D-14-0106.1

816

817 Rana, S., McGregor, J., and Renwick, J.: Dominant modes of winter precipitation variability over
818 Central Southwest Asia and inter-decadal change in the ENSO teleconnection, Climate dynamics,
819 53, 5689-5707, 2019. https://doi.org/10.1007/s00382-019-04889-9

820

821 Ridley, J., Wiltshire, A., and Mathison, C.: More frequent occurrence of westerly disturbances in
822 Karakoram up to 2100, Science of the Total Environment, 468, S31-S35, 2013.
823 http://dx.doi.org/10.1016/j.scitotenv.2013.03.074

824

825 Schneider, U., Becker, A., Finger, P., Meyer-Christoffer, A. and Ziese, M.: GPCC full data monthly
826 product version 2018 at 0.25: monthly land-surface precipitation from rain-gauges built on GTS-
827 based and historical data, Global Precipitation Climatology Centre, 2018.

828

829 Singh, T., Saha, U., Prasad, V. S., and Gupta, M. D.: Assessment of newly-developed high
830 resolution reanalyses (IMDAA, NGFS and ERA5) against rainfall observations for Indian region,
831 Atmospheric Research, 259, 105679, 2021. https://doi.org/10.1016/j.atmosres.2021.105679

832

833 Syed, F. S., Giorgi, F., Pal, J. S., and Keay, K.: Regional climate model simulation of winter climate
834 over Central-Southwest Asia, with emphasis on NAO and ENSO effects, International journal of
835 climatology, 30(2), 220-235, 2010. DOI: 10.1002/joc.1887

836

837 Tahir, A. A., Chevallier, P., Arnaud, Y., and Ahmad, B.: Snow cover dynamics and hydrological
838 regime of the Hunza River basin, Karakoram Range, Northern Pakistan, Hydrology and Earth
839 System Sciences, 15(7), 2275-2290, 2011. https://doi.org/10.5194/hess-15-2275-2011

840

841 Wang, L., Chen, W., Zhou, W., and Huang, R.: Interannual variations of East Asian trough axis at
842 500 hPa and its association with the East Asian winter monsoon pathway, Journal of Climate, 22(3),
843 600-614,2009. https://doi.org/10.1175/2008JCLI2295.1

844

845 Wang, S., Huang, J., He, Y., and Guan, Y.: Combined effects of the Pacific decadal oscillation and
846 El Nino-southern oscillation on global land dry–wet changes, Scientific reports, 4(1), 6651, 2014.
847 DOI: 10.1038/srep06651

848

849 Wang, W., Matthes, K., Omrani, N. E., and Latif, M.: Decadal variability of tropical tropopause
850 temperature and its relationship to the Pacific Decadal Oscillation, Scientific reports, 6(1), 29537,
851 2016. DOI: 10.1038/srep29537

852

853 Wang, X., Tolksdorf, V., Otto, M., and Scherer, D.: High Asia Refined Analysis Version 2 (HAR
854 v2): a New Atmospheric Data Set for the Third Pole Region, EGU General Assembly Conference
855 Abstracts (p. 8756), 2020. DOI: 10.5194/egusphere-egu2020-8756

856

857   Wester, Philippus, Mishra, Arabinda, Mukherji, Aditi, Shrestha, Arun Bhakta (Eds.),: The Hindu
858   Kush Himalaya Assessment: Mountains, Climate Change, Sustainability and People, Springer,
859   HIMAP, 2020.

860

861   Wittenberg, A. T., Rosati, A., Delworth, T. L., Vecchi, G. A., and Zeng, F.: ENSO modulation: Is it
862   decadally predictable?, Journal of Climate, 27(7), 2667-2681, 2014. https://doi.org/10.1175/JCLI-
863   D-13-00577.1

864

865   Wu, B., and Wang, J.: Winter Arctic oscillation, Siberian high and East Asian winter monsoon,
866   Geophysical research letters, 29(19), 3-1, 2002. https://doi.org/10.1029/2002GL015373

867

868   Wu, X., and Mao, J.: Interdecadal modulation of ENSO-related spring rainfall over South China by
869   the Pacific Decadal Oscillation, Climate dynamics, 47, 3203-3220, 2016. DOI 10.1007/s00382-016-
870   3021-y

871

872   Xie, P., and Arkin, P. A.: Global precipitation: A 17-year monthly analysis based on gauge
873   observations, satellite estimates, and numerical model outputs, Bulletin of the american
874   meteorological society, 78(11), 2539-2558, 1997. https://doi.org/10.1175/1520-
875   0477(1997)078%3C2539:GPAYMA%3E2.0.CO;2

876

877   Yadav, R. K., Rupa Kumar, K., and Rajeevan, M.: Increasing influence of ENSO and decreasing
878   influence of AO/NAO in the recent decades over northwest India winter precipitation, Journal of
879   Geophysical Research: Atmospheres, 114(D12), 2009. doi:10.1029/2008JD011318

880

881   Yadav, R. K., Yoo, J. H., Kucharski, F., and Abid, M. A.: Why is ENSO influencing northwest India
882   winter precipitation in recent decades?, Journal of Climate, 23(8), 1979-1993, 2010. DOI:
883   10.1175/2009JCLI3202.1

884

885 Yadav, R. K., Rupa Kumar, K., and Rajeevan, M.: Role of Indian Ocean sea surface temperatures in

886 modulating northwest Indian winter precipitation variability, Theor. Appl. Climatol., 87, 73-83,

887 2007. DOI 10.1007/s00704-005-0221-5

888

889 Yamagami, Y., and Tozuka, T.: Interdecadal changes of the Indian Ocean subtropical dipole mode,

890 Clim Dyn, 44, 3057-3066, 2015. DOI 10.1007/s00382-014-2202-9

891

892 Yang, Q., Ma, Z., and Xu, B.: Modulation of monthly precipitation patterns over East China by the

893 Pacific Decadal Oscillation, Climatic change, 144, 405-417, 2017. DOI: 10.1007/s10584-016-1662-

894 9

895

896 Yatagai, A., Kamiguchi, K., Arakawa, O., Hamada, A., Yasutomi, N., and Kitoh, A.: APHRODITE;

897 Constructing a long-term daily gridded precipitation dataset for Asia based on a dense network of

898 rain gauges, Bulletin of the American Meteorological Society, 93(9), 1401-1415, 2012.

899 https://doi.org/10.1175/BAMS-D-11-00122.1

900

901 Yin, J., and Zhang, Y.: Decadal changes of East Asian jet streams and their relationship with the

902 mid-high latitude circulations, Climate Dynamics, 56, 2801-2821, 2021.

903 https://doi.org/10.1007/s00382-020-05613-8

904

905 Yuan, X., Yang, K., Lu, H., He, J., Sun, J., and Wang, Y.: Characterizing the features of precipitation

906 for the Tibetan Plateau among four gridded datasets: Detection accuracy and spatio-temporal

907 variabilities, Atmospheric Research, 264, 105875, 2021.

908 https://doi.org/10.1016/j.atmosres.2021.105875

909

910 Zhang, Y., Wallace, J. M., and Battisti, D. S.: ENSO-like interdecadal variability: 1900–93, Journal

911 of climate, 10(5), 1004-1020, 1997. https://doi.org/10.1175/1520-0442(1997)010%3C1004:ELIV

912 %3E2.0.CO;2

913

914 Zhang, R., and Delworth, T. L.: Impact of the Atlantic multidecadal oscillation on North Pacific

915 climate   variability,   Geophysical   Research   Letters,   34(23),   2007.

916 https://doi.org/10.1029/2007GL031601